Structures and Dynamic Motion of Laminin-1 As Observed by Atomic Force Microscopy†

Christine H. Chen,‡ Dennis O. Clegg,§ and Helen G. Hansma*,‡

Department of Physics and Neuroscience Institute and Department of Molecular, Cellular, and Developmental Biology, University of California, Santa Barbara, California 93106

Received December 17, 1997; Revised Manuscript Received April 6, 1998

ABSTRACT: Laminins are a family of multifunctional extracellular matrix glycoproteins that play important roles in the development and maintenance of tissue organization via their interactions with cells and other extracellular matrix proteins. To understand the structural basis of laminins' functions, we examined the motion of laminin-1 (Ln-1) in physiological buffers using atomic force microscopy. While many Ln-1 molecules assumed the expected cruciform structure, unexpected dynamic movements of the Ln-1 arms were observed in aqueous environments. These dynamic movements of the Ln-1 arms may contribute to the diversity of laminin functions.

Laminins are a family of extracellular matrix proteins that support cell−matrix interactions thought to be crucial for the movement and differentiation of a variety of cell types during development. Laminin-1 (Ln-1; EHS laminin),[1] the first laminin to be discovered, is a large (900 kDa) cruciform-shaped basement membrane glycoprotein (*1*−*4*) composed of three different polypeptide chains: α (400 kDa), *β* (220 kDa), *γ* (200 kDa) (*5*). Laminin plays an important role in stimulating growth and differentiation of various cell types, supports cell migration and cell adhesion, induces polarity in epithelial cells, organizes the basement membrane, and promotes neurite outgrowth (*2*, *6*−*11*). Because of its importance in the development and maintenance of cellular organization, it is important to determine which Ln-1 structures give rise to its many functions.

Previous studies of laminin using electron microscopy were done by flattening the specimen onto a support and adding metals to achieve either negative or positive staining (*12*, *13*). Analyzing biological specimens with the electron microscope is challenged by many limiting factors. Staining methods for electron microscopy are done at concentrations and pH values that are far from physiological. The specimens are likely to be damaged and distorted by the electron radiation, metal staining methods, and rotary-shadowing methods. Furthermore, all mobility and three-dimensional arrangement are lost due to the adsorption of sample to the hard support (*13*).

In this study, we investigated the three-dimensional arrangement and dynamic motion of Ln-1 molecules utilizing atomic force microscopy (AFM, also known as SFM, scanning force microscopy). AFM has become a powerful research tool in molecular biology in recent years (*14*−*17*). The atomic force microscope (AFM) images sample surfaces by raster scanning a sharp tip across the sample surface. The tip is on the end of a flexible cantilever that detects angstrom-sized changes in the heights of the surface features to give the topographic information about the surface of the molecule (*18*−*20*).

AFM is a good alternative to electron microscopy for determining the structures of biomolecules. One of the most distinguished features of the AFM is its ability to observe molecules in three dimensions even in physiological solutions, when the molecules are on flat surfaces.

MATERIALS AND METHODS

Reagents. Mouse laminin (1 mg/mL) purified from EHS sarcoma tissue was purchased from Gibco-BRL (Grand Island, NY). The laminin was stored at −80 °C and diluted with different buffers (see below) to the desired concentrations.

Buffers. Four different buffers at pH 7.4 were used: high-salt MOPS buffer (20 mM MOPS, 5 mM $MgCl_2$, 150 mM NaCl), low-salt MOPS buffer (20 mM MOPS, 25 mM NaCl, 5 mM $MgCl_2$, pH 7.4), PBS in 5 mM $MgCl_2$ (10 mM phosphate buffer, 2.7 mM KCl, 137 mM NaCl; PBS tablets, Sigma Chemical, St. Louis, MO), and Tris buffer (50 mM Tris, 150 mM NaCl, 5 mM $MgCl_2$).

Sample Preparations. Disks of mica (Ruby Muscovite mica; New York Mica Co., New York, NY) were glued to steel disks with 2-Ton epoxy (Devcon Corp., Wood Dale, IL) and allowed to dry overnight or longer. The dried mica disks were cleaved with Scotch tape immediately before use.

For AFM in Air. Ln-1 (1 mg/mL) was diluted in PBS (0.1−0.01 μg/μL final concentrations), and approximately 10 μL of diluted Ln-1 was pipetted onto freshly cleaved mica.

† This work was supported by NSF Grant MCB 9604566 (H.G.H), U. S. Army Research Office Multidisciplinary University Research Initiative DAAH04-96-1-0443 (C.H.C), NIH Grant EY09736 (D.O.C), and Digital Instruments.

* To whom correspondence should be addressed.

‡ Department of Physics.

§ Neuroscience Institute and Department of Molecular, Cellular, and Developmental Biology.

[1] Abbreviations: AFM, atomic force microscope/microscopy; SFM, scanning force microscope/microscopy; Ln-1, laminin-1, EHS laminin; ECM, extracellular matrix; PBS, phosphate-buffered saline; α, α_1 peptide chain of Ln-1; *β*, β_1 peptide chain of Ln-1;*γ*, γ_1 peptide chain of Ln-1; EBD, electron-beam deposited.

S0006-2960(97)03097-3 CCC: $15.00
Published on Web 05/15/1998

The sample was left on the mica for about 10 s before being washed off with Milli-Q purified water (Millipore Corp., Bedford, MA) and then dried immediately with compressed air. The sample was further dried in a vacuum desiccator over P_2O_5.

For AFM in Liquid. Ln-1 samples (0.002−0.01 μg/μL) were prepared with different buffers. The samples were loaded onto the mica in two ways. First, about 35−40 μL was pipetted onto freshly cleaved mica and left in a tightly sealed Petri dish filled with water overnight. The micas were washed with Milli-Q water the next day and imaged in both water and buffers by adding about 100−150 μL of liquid directly onto the washed mica. In the second way, a Pap Pen (Electron Microscopy Sciences, Ft. Washington, PA) was used to create a hydrophobic boundary on the mica so that the sample (30−40 μL) stayed in a droplet form overnight. In this way, we could use a smaller sample volume. The micas were washed with Milli-Q water the next day and imaged in buffers.

AFM Imaging. All data were gathered on a Nanoscope III with a Multi Mode AFM (Digital Instruments, Santa Barbara, CA). D and E scanners were used, which have maximum scan sizes of 10−15 μm, and were calibrated to ca. 8% in the *xy* direction. Scan rates ranged from 6 to 8 Hz, and tapping frequencies ranged from 10 to 20 kHz in fluid and 250−270 kHz in air. All air sample images were captured with 100 μm silicon cantilevers (Digital Instruments) in air or in a helium chamber. Narrow 100-μm silicon−nitride cantilevers (Digital Instruments) were modified under an electron beam (EBD) for liquid sample imagings. Images were processed by flattening to remove the background slope.

RESULTS

The structures of Ln-1 molecules were studied by AFM in both air and liquid. Consistent with previous studies of Ln-1 by the electron microscopy (*1*, *4*, *13*, *21*), we observed many cross-shaped or cruciform molecules. In addition, we observed Ln-1 molecules with many other shapes (Figure 1). Only the well-extended Ln-1 molecules appear cross-shaped. Other Ln-1 molecules attach to the mica surface in random configurations forming X, Y, or T shapes with three or four appendages. Three short arms and one long arm of well-extended Ln-1 are measured to be approximately 49 ± 6 and 76 ± 11 nm, respectively. The short arms are named as in the inset of Figure 1.

The variety of images observed suggest that flexible Ln-1 arms are capable of various degrees of bending and folding (Figure 1). Additionally, short but thick arms of some molecules (Figure 1D,J) suggest that arms can fold over upon themselves to reduce their lengths and increase their heights. These overlapped arms are 2.3 ± 0.32 nm high, as compared to 0.68 ± 0.08 nm of regular arms. Moreover, we can clearly observe the inner and the end globular units of the γ and β short arms (Figure 1A−G,I,K) as seen by bright spots in the arms. Although these globules appear as the same sizes, the end unit is slightly higher (1.43 ± 0.18 nm) than the inner unit (1.3 ± 0.2 nm). The end globular unit of the α arm seems to be shorter (1.1 nm) than the two inner units, which have similar heights as those of the γ and β arms

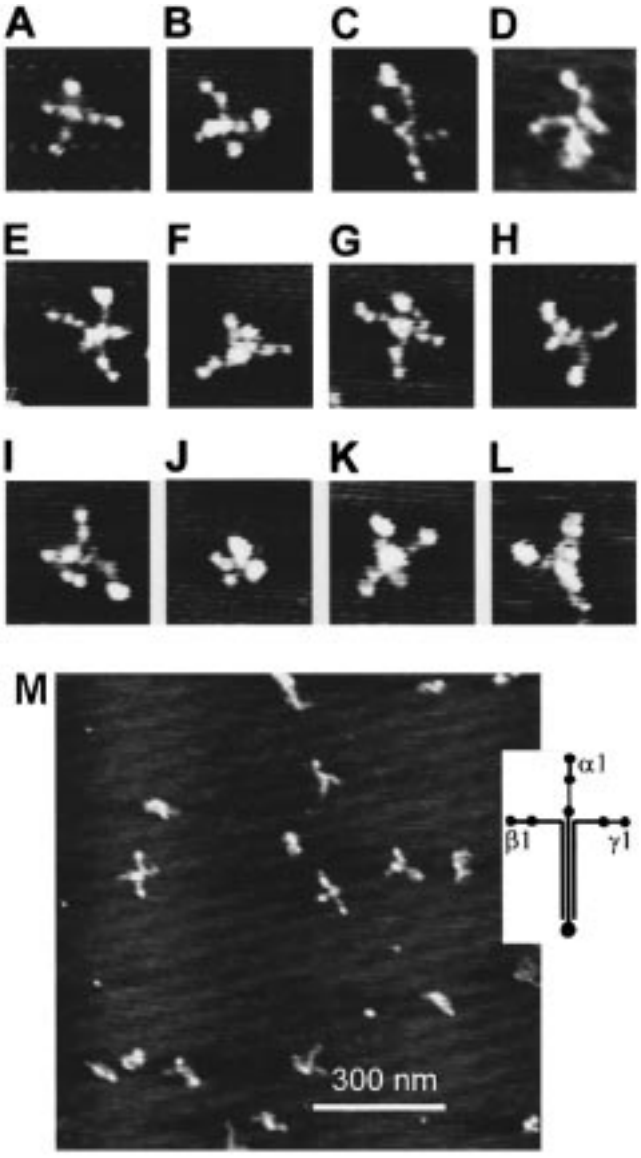

FIGURE 1: Height images of Ln-1 molecules observed by AFM in air. Images (A−L) show different orientations and conformations of individual Ln-1 molecules. Image M shows a typical field of Ln-1 molecules; the inset shows the schematic structure of Ln-1 (6). Notice that globular units can be seen as bright spots on the arms. The highest points (the brightest spots) are most likely to be the globular unit of the long arm (C, E, H, I); however, they may also be the overlap of the arms in other cases (J, K, L). The sizes of the images are 140 nm × 140 nm for panels A−L and 1.1 μm × 1.1 μm for panel M.

(1.3 nm). The brightest spot at the end of each long arm (Figure 1C,E,G,I) is the globular unit of the long arm; these are approximately 2.15 ± 0.2 nm high. Therefore, one may assume that the height of overlapped regions (2.3 ± 0.18 nm) results from the folding of regular regions or the overlapping of a regular region (0.68 nm) with a globular region (1.3−1.4 nm).

Furthermore, the arms of Ln-1 molecules project outward as if they originate from a single point in the molecule. The orientations of the arms seem to center around this point of attachment where all four arms intersect. The random arrangements of molecules are not due to sample preparation artifacts such as blow-drying with air, because this variety of shapes is observed consistently throughout every sample. Also, the molecules show a random orientation on the mica

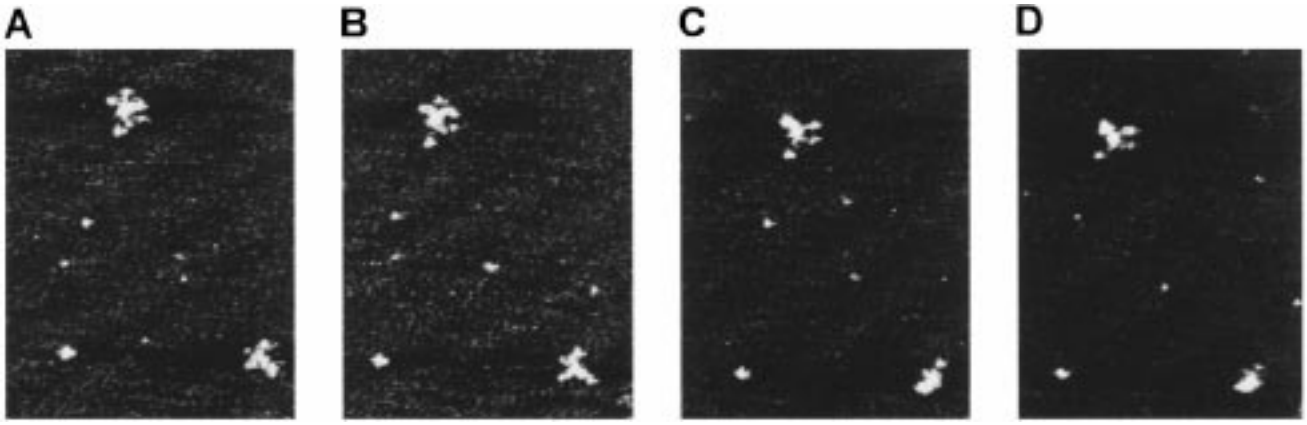

FIGURE 2: Sequential height images of two Ln-1 molecules in a low-salt MOPS buffer, showing the movement of arms, especially for the lower molecule. All images are 420 nm × 540 nm.

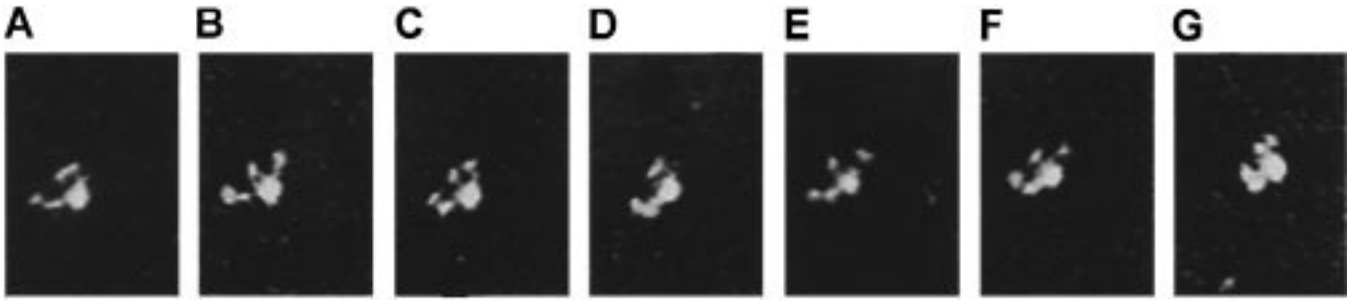

FIGURE 3: Motion and interaction of Ln-1 arms in a high-salt MOPS buffer (20 mM Mops, 5 mM $MgCl_2$, 150 mM NaCl). These height images were captured sequentially, but the time elapsed between images varied (1.2−4.8 min). The arms of the molecule in this figure seem to overlap in the center, giving rise to a high spot in the center of the molecule, and they tend to move around this central blob. All images are 140 nm × 200 nm.

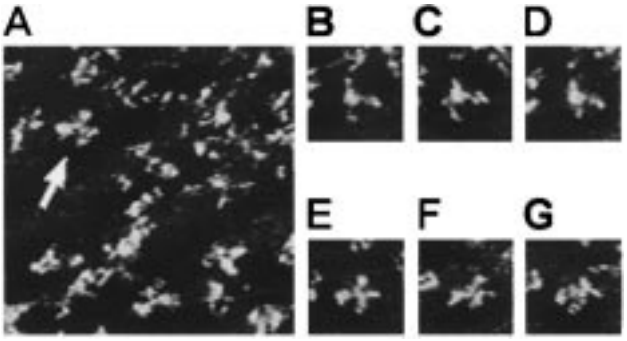

FIGURE 4: Dense field of moving Ln-1 molecules in a high-salt MOPS buffer, showing the difficulty of imaging (A). Panels B−F are sequential images showing movement of the Ln-1 molecule indicated by the arrow in panel A. AFM height images are 420 nm × 420 nm (A) and 140 nm × 140 nm (B−F).

surface and not a directional orientation as seen in elongated molecules that are oriented by the blow-drying in a particular way. The Ln-1 arms do not move during repeated imaging in air.

Imaging in liquid enabled us to observe dynamic motions of Ln-1 molecules, thus lending support to the theory of arm flexibility arising from the images observed by AFM in air. Of the four different buffers that we used for imaging, the two MOPS buffers (low salt and high salt) were the best for imaging substructures in individual Ln-1 molecules (Figures 2−6). Figure 2 shows a movie of Ln-1 molecules in the low-salt MOPS buffer. Image acquisition times are typically 45 s/image. Notice how the shape of the molecule at the lower right-hand corner changed as time elapsed. It started out somewhat T-shaped (Figure 2A), then became more cross-shaped (Figure 2B), and lost its arms eventually and balled up (Figure 2D) as its arms moved around in the buffer. The arms appear to move randomly in fluid, resulting in unpredictable structures, and it is also not certain that molecules would go back to the shapes with which they started out in a given amount of time.

The random arm movements of Ln-1 molecules were also observed in high-salt MOPS buffers (ca. 150 mM, which is a physiological concentration; Figures 3−6). In Figure 3, the arms spread out, bend, fold, and contract to give the molecule different conformations. This figure vividly shows the flexibility and mobility of Ln-1 arms in a physiological buffer.

As previously described, it seems as if there is a central point in the molecule where the arms meet and where the molecule is anchored to the surface of the mica. The mica binding site may be near one of the cell attachment sites of the Ln-1 molecule, such as domain III of β_1 chain (*1*) or fragment 1 (*24*, *25*), which are in the vicinity of the arm intersection. While we observed various movements of Ln-1 arms in buffer, we never saw individual Ln-1 molecules move to different locations on the mica surface.

Imaging in a high-salt buffer is not as easy as imaging in a low-salt buffer. Generally, the images appear less well-defined in high salt, perhaps because the Ln-1 molecules are more weakly attached to the mica (Figure 4). However, even under these conditions, some well-defined Ln-1 molecules could be identified. We selected an individual molecule of a field (A, arrow) to demonstrate the persistent, dynamic motion of laminin in a physiological buffer (Figure 4B−G). As observed before, the arms retract and spread

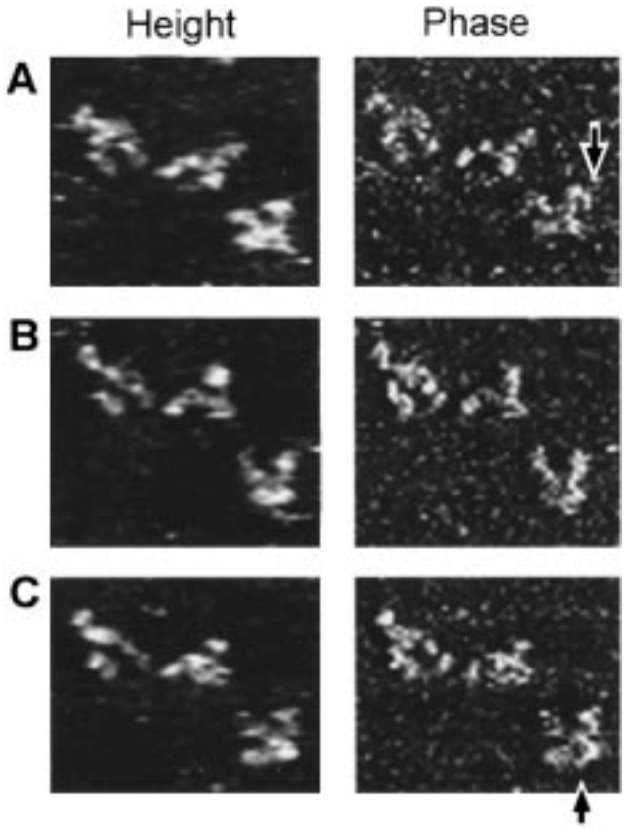

FIGURE 5: Details in moving Ln-1 molecules can be seen in AFM phase images (right). A few molecules from the same field are shown in panels A−C in both height (left) and phase (right) images. Phase imaging provides additional information that is difficult or impossible to detect in the height mode (A, C, arrows). The images in panels A−C are 280 nm × 210 nm.

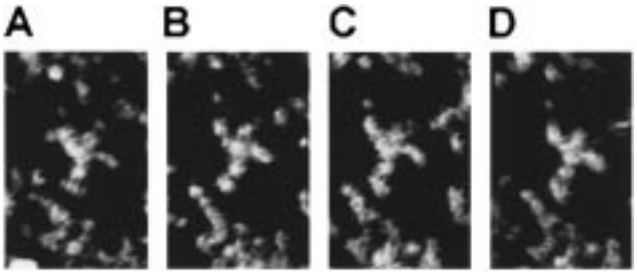

FIGURE 6: Sequential images of a relatively stable Ln-1 molecule in a high-salt MOPS buffer. While arm movements are seen in most Ln-1 molecules in aqueous environments, some molecules such as this one show the stability and immobility of its arms. These height images are 150 nm × 230 nm.

randomly to give the Ln-1 molecules different shapes over time.

AFM phase images sometimes show substructures in the Ln-1 arms that are not visible in height images (Figure 5, arrows). Phase images in tapping AFM show the phase difference between the oscillation driving the cantilever and the oscillation of the cantilever as it interacts with the sample surface (*26*−*29*). In air, phase images are a measure of the energy dissipated by the tip−sample interaction (*30*). The degree of adhesion between the tip and the sample correlates with the darkness in the phase image, if the tip is imaging at a force high enough to produce a repulsive interaction with the surface. The cantilever oscillation in air is sinusoidal, while in liquid the harmonica of cantilever motion

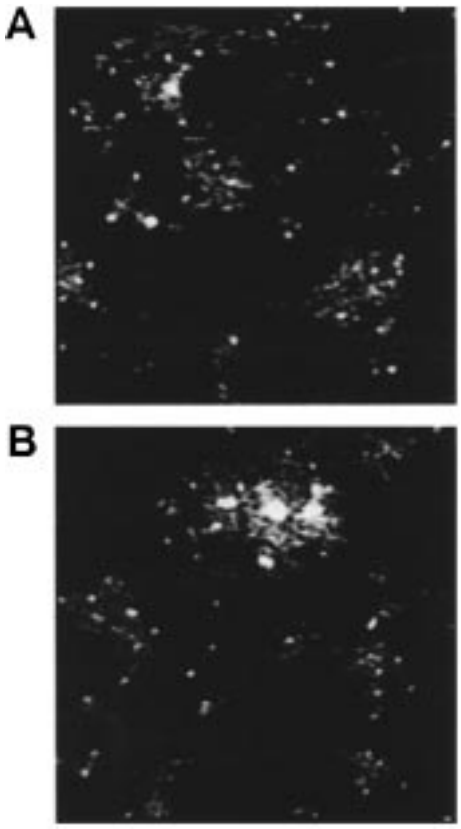

FIGURE 7: Height images of Ln-1 in Tris buffer (A) and PBS (B). Images are 1 μm × 1 μm.

are more complex. Therefore, the interpretation of phase images in liquid is also more complex. It is quite possible, however, that for phase images in liquid the dark regions are also more adhesive than the light regions. Mica, which is generally more adhesive than biomolecules (*15*, *31*), is darker in these phase images than the bulk of the Ln-1 molecules. Therefore, the substructures in phase images of Ln-1 (Figure 5, arrows) may be regions of the Ln-1 arms that have greater and lesser adhesion to the AFM tip.

While some laminin molecules exhibit dynamic motion in an aqueous environment, other laminin molecules are relatively stable (Figure 6). In contrast to other Ln-1 molecules in liquid, this Ln-1 molecule showed only small changes in the conformations of the arms, especially the two sidearms. Although it is not certain whether the immobility is due to better adhesion of the molecule to the mica, or simply a more stable conformation of the molecule, this shows that the motions we observed earlier are not solely due to the tip artifacts.

The other two buffers used in this study, Tris and PBS, were not good for imaging with AFM in liquid. The Ln-1 molecules tended to aggregate in these buffers, and the images showed streaks typical of poorly bound molecules (Figure 7). Since it was hard to image individual molecules, these buffers were not used in further studies.

DISCUSSION

Recently the extracellular matrix (ECM) has captured the attention and interest of cell biologists and molecular biologists, as it has become clear that the ECM plays an active role in tissue development and maintenance. Laminins are major ECM components that have important influences

on both normal and cancer cells (*2*, *3*, *10*, *23*, *32*, *33*). Previous studies suggest that strong interactions between laminin and invasive tumor cells enhance the metastatic propensity of the tumor cells by allowing them to cross the basement membrane more readily. In addition, the interactions of laminin with ECM components and the laminin−laminin interactions play important roles in matrix organization (*21*, *22*, *34*).

To understand how laminin is capable of playing these multiple roles during development, it is essential to determine its structure−function relationships. Our study shows that Ln-1 molecules have freely moving arms with an ability to change their structures dynamically in aqueous environments and provides possible insights into how Ln-1 carries out its multiple functions. Arm movement may control the accessibility of cells and ECM molecules to binding sites on the Ln-1 cruciform. For example, interactions between Ln-1 and other proteins may bend Ln-1 arms to cover or expose cell-binding sites. In addition, the arm movement may influence or direct the end-to-end self-assembly interactions of laminin molecules.

The mobility of Ln-1 arms in the AFM may be caused by reversible adsorption and release from the mica surface, possibly due to their thermal energy. There may have been some tip-induced motion, but our study illustrates that Ln-1 molecules are stable and flexible enough to produce such motions in an aqueous environment.

In previous studies of structure−function relationships of Ln-1, molecular biologists have assigned various functions of laminin to different domains on the molecule by using proteolytic fragmentation methods and synthetic peptides (*1*, *23*, *35*−*37*). However, there are limitations to using synthetic peptides. Not all parts of laminin are available for defined fragments, and prepared small fragments do not necessarily retain native conformation; thus, they are likely to differ in some ways from the functions of native laminin (*1*). Therefore, it is a challenge to construct a suitable assay system to test the functions of distinct regions. Our results suggest that AFM will prove useful to assay the molecular dynamics of laminins.

In the future, we plan to determine how Ln-1-binding molecules such as nidogen/entactin, collagen IV, and heparan sulfate proteoglycan affect the dynamic arm movement. In addition, the AFM can measure intermolecular and intramolecular forces by pulling on the molecules (*38*−*42*) in force mapping methods. By taking advantage of this powerful ability of AFM, we plan to investigate the affinity of Ln-1 for its various substrates and cell receptors by using force mapping techniques. These approaches to the understanding of structure/function relationships and physical properties of laminin will facilitate our understanding of the biology of laminin molecules during development.

ACKNOWLEDGMENT

We thank Paul Hansma and Dan Morse for their generous assistance in support of this research, Tilman Schaffer for technical assistance, and Scott Hansma for developing tiff conversion software.

REFERENCES

1. Beck, K., Hunter, I., and Engel, J. (1990) *FASEB J. 4*, 148−160.
2. Martin, G., and Timpl, R. (1987) *Annu. Rev. Cell Biol. 3*, 57−85.
3. Timpl, R., Engel, J., and Martin, G. R. (1983) *Trends Biochem. Sci. 8*, 207−209.
4. Engel, J., Odermatt, E., and Engel, A. (1981) *J. Mol. Biol. 150*, 97−120.
5. Burgeson, R. E., Chiquet, M., Deutzmann, R., Ekblom, P., Engel, J., Kleinman, H., Martin, G. R., Meneguzzi, G., Paulsson, M., Sanes, J., Timpl, R., Yamada, K. T., and Yurchenco, P. D. (1994) *Matrix Biol. 14*, 209−211.
6. Timpl, R., and Brown, J. (1994) *Matrix Biol. 14*, 275−281.
7. Johansson, S., Kjellen, L., Hook, M., and Timpl, R. (1981) *J. Cell Biol. 90*, 260−264.
8. Kleinman, H., Cannon, F., Laurie, G., Hassell, J., Aumailley, M., Terranova, V., Martin, G., and DuBois-Dalcq, M. (1985) *J. Cell. Biochem. 27*, 317−325.
9. Manthorpe, M., Engvall, E., Ruoslahti, E., Longo, F., Davis, G., and Varon, S. (1983) *J. Cell Biol. 97*, 1882−1890.
10. Terranova, V., Rao, C., Kalebic, T., Margulies, I., and Liotta, L. (1983) *Proc. Natl. Acad. Sci. U.S.A. 80*, 444−448.
11. Rizzino, A., Terranova, V., Rohrbach, D., Crowley, C., & Rizzino, H. (1980) *J. of Supramol. Struct. 13*, 243−253.
12. Paulsson, M., Aumailley, M., Deutzmann, R., Timpl, R., and Beck, K. E. J. (1987) *Eur. J. Biochem. 166*, 11−19.
13. Engel, J., and Furthmayr, H. (1987) *Extracell. Matrix Compon. 145*, 3−78.
14. Shao, Z., Mou, J., Czaijkowsky, D. M., Yang, J., and Yuan, J.-Y. (1996) *Adv. Phys. 45*, 1−86.
15. Hansma, H. G. (1996) *J. Vac. Sci. Technol., B 14*, 1390−1394.
16. Bustamante, C., and Keller, D. (1995) *Phys. Today 48*(12), 32−38.
17. Hansma, H. G., and Hoh, J. (1994) *Annu. Rev. of Biophys. Biomol. Struct. 23*, 115−139.
18. Quate, C. F. (1994) *Surf. Sci. 299/300*, 980−995.
19. Rugar, D., and Hansma, P. K. (1990) *Phys. Today 43*(10), 23−30.
20. Binnig, G., Gerber, C., Stoll, E., Albrecht, R. T., and Quate, C. F. (1987) *Europhys. Lett. 3*, 1281−1286.
21. Yurchenco, P. D., and O'Rear, J. (1993) in *Molecular and Cellular Aspects of Basement Membranes* (Rohrbach, D. H., and Timpl, R., Eds.) pp 19−47, Academic Press, Inc., San Diego, CA.
22. Timpl, R. (1989) *Eur. J. Biochem. 180*, 487−502.
23. Timpl, R., and Rohde, H. (1979) *J. Biol. Chem. 254*(19), 9933−9937.
24. Timpl, R., Johansson, S., vanDelden, V., Oberbaumer, I., and Hook, M. (1983) *J. Biol. Chem. 258*, 8922−8927.
25. Rao, C. N., Margulies, I. M. K., Tralka, T. S., Terranova, V. P., Madri, J. A., and Liotta, L. A. (1982) *J. Biol. Chem. 257*, 9740−9744.
26. Magonov, S. N., Elings, V., and Whangbo, M.-H. (1997) *Surf. Sci. 375*, 385−391.
27. Argaman, M., Golan, R., Thomson, N. H., and Hansma, H. G. (1997) *Nucleic Acids Res. 25*, 4379−4384.
28. Hansma, H. G., Kim, K. J., Laney, D. E., Garcia, R. A., Argaman, M., and Parsons, S. M. (1997) *J. Struct. Biol. 119*, 99−108.
29. Babcock, K. L., and Prater, C. B. (1995) Digital Instruments, Santa Barbara, CA.
30. Cleveland, J. P., Anczykowske, B., Schmid, A. E., and Elings, V. B. (1998) *Appl. Phys. Lett.* (in press).
31. Radmacher, M., Cleveland, J. P., Fritz, M., Hansma, H. G., and Hansma, P. K. (1994) *Biophys. J. 66*, 2159−2165.
32. Terranova, V., Liotta, L., Russo, R., and Martin, G. (1982) *Cancer Res. 42*, 2265−2269.
33. Travis, J. (1997) *Sci. News 152*, 138−139.
34. Kleinman, H. K., McGarvey, M. L., Hassell, J. R., Star, V. L., Cannon, F. B., Laurie, G. W., and Martin, G. R. (1986) *Biochemistry 25*, 312−318.
35. Graf, J., Iwamoto, Y., Sasaki, M., Martin, G., Kleinman, H., Robey, F., & Yamada, Y. (1987) *Cell 48*, 989−996.
36. Timpl, R., and Dziadek, M. (1986) *Int. Rev. Exp. Pathol. 29*, 1−112.

37. Ott, U., Odermatt, E., Engel, J., Furthmayr, H., and Timpl, R. (1982) *FEBS Lett. 123*, 63−72.
38. Rief, M., Gautel, M., Oesterhelt, F., Fernandez, J. M., and Gaub, H. E. (1997) *Science 276*(5315), 1109−112.
39. Rief, M., Oesterhelt, F., Heymann, B., and Gaub, H. E. (1997) *Science 275*(5304), 1295−1297.
40. Dammer, U., Popescu, O., Wagner, P., Anselmetti, D., Guentherodt, H.-J., and Misevic, G. N. (1995) *Science 267*, 1173−1175.
41. Lee, G. U., Chrisey, L. A., and Coulton, R. J. (1994) *Science 266*, 771−773.
42. Moy, V. T., Florin, E.-L., and Gaub, H. E. (1994) *Science 266*, 257−259.

BI973097J